Quantitative InfraRed Thermography, 2016
http://dx.doi.org/10.1080/17686733.2015.1102475

Taylor & Francis
Taylor & Francis Group

Weld pool surface temperature measurement from polarization state of thermal emission

Nicolas Coniglio[a], Alexandre Mathieu[b]*, Olivier Aubreton[c] and Christophe Stolz[c]

[a]*Laboratoire MSMP, Arts et Metiers ParisTech, Aix en Provence, France;* [b]*Laboratoire Interdisciplinaire Carnot de Bourgogne (ICB), UMR 6303 CNRS-Université de Bourgogne Franche-Comté, Dijon, France;* [c]*Laboratoire LE2I, UMR 6306 CNRS-Université de Bourgogne Franche-Comté, Le Creusot, France*

(*Received 29 October 2014; accepted 22 September 2015*)

This paper presents a passive polarimetry method using a division of aperture optical device in order to measure the temperature distribution at the weld pool surface. Thermal emission from a hot liquid metal was investigated at a near-infrared wavelength corresponding to a blind spectral window of a helium plasma generated during gas tungsten arc welding process. The refractive index of liquid metal and the surface radiance are deduced from the polarisation state of thermal emissions. Based upon the knowledge of both characteristics, the temperature distribution can be calculated.

Keywords: polarimetry; Stokes imaging; gas tungsten arc; weld pool temperature

1. Introduction

Vision-based methods are one of the non-contact solutions to provide insights on the state of the weld pool surface hidden by the bright dazzling radiations of the welding arc. The welding arc plasma emits radiations at specific spectral lines,[1] the wavelengths of which are mainly determined by the shielding gas composition and the atoms evaporated from the weld pool during its interaction with the arc plasma. Observing the weld pool at a specific wavelength reduces the interference from the arc and facilitates the observation of the weld pool area behind the arc plasma.[2–4] While thermal emission intensity is related to the temperature of the emitting surface, the inter-dependence of the surface geometry and the observing setup is usually neglected. However, the emissivity of thermal radiation from an object depends upon both the angle of emission relative to the surface [5] and the surface temperature.[6]

Measurement of weld pool temperature is a real challenge for scientific research but also for industrial applications. Non-contact methods are commonly preferred to contact methods due to difficulties related to the environment: high temperature, molten metal spatters, intense radiation, dazzling effect, small scale and short time phenomena. Attempts to measure superficial temperature of the weld pool exist in literature review. Most of this works concerns feasibility studies of IR thermography sensing with the aim to control cooling rate near the weld pool,[7–14] for detecting contaminant/impurities on the molten pool surface,[15] for penetration sensing,[16, 17] or for monitoring the size

*Corresponding author. Email: alexandre.mathieu@u-bourgogne.fr

of the weld pool.[18] Few works concerns absolute temperature measurement on the weld pool surface. Among them, authors of [4] use IR thermography and assume a direct dependence between pixel grey levels and temperature. Authors of [19–23] use two-colour pyrometers to measure weld pool temperature, assuming an emissivity independent from wavelength. Others [24, 25] use optical emission spectroscopy to determine a relation between emissivity and temperature. Then, they use this relation with IR image to calculate a temperature map on weld pool surface. From our knowledge, the only authors that do not neglect directionality of thermal emission coming from the weld pool surface are Kraus et al. [26, 27], who take into account for surface topology of the weld pool and optical axis angle of view. However, the Kraus method is difficult to achieve and is applicable only when the welding arc vanishes.

In the first part of this article, the principle of Stokes polarimetric analysis is reminded. Extension of this method to temperature measurement of weld pool surface is proposed assuming four initial postulates. The method used to determine the complex refractive index is emphasised as it represents a key point of the proposed method. In the experimental part, description of the set-up is given. In the discussion part, the method and the results are discussed. An interpretation of the observed scene is proposed.

2. Thermal radiation polarimetric analysis

From [28], body thermal emissions are linearly polarised parallel to the plane of incidence for objects presenting a particular aspect ratio, e.g. wire or fibre. In the present work, the local surface orientation is deduced from the polarimetric analysis of the near-infrared radiations emitted by a weld pool composed of liquid steel. A complex refractive index is estimated and, then, local temperature is calculated. Four initial postulates are proposed to determine the temperature distribution:

- The weld pool edge is at the liquidus temperature, due to undercooling phenomenon, temperature variation of several degrees can be observed at the weld pool edge. In the works set out in this article, the weld pool is observed in stationary condition, thus, reducing overcooling temperature variation at the weld pool edge.
- The emissivity of liquid iron at $\theta = 0°$ is assumed wavelength-independent in the 650–810 nm range, which enables to use values at 650 nm [29]: ε ($\theta = 0°$, $\lambda = 810$ nm) $= \varepsilon$ ($\theta = 0°$, $\lambda = 650$ nm) $= 0.37$.
- The weld pool radiance is related to the blackbody radiance at the same temperature by the Planck law.
- The liquid metal emissivity is independent of its temperature for the temperature range investigated.

In opposite to some works in the close field,[30–32] thermal radiations are body emissions that can be partially linearly polarised in the far field,[33–37] but to a degree of linear polarisation usually less than for surface reflection.[38] The degree of linear polarisation depends upon the zenithal angle of the emitted radiation following a change in emissivity with the direction of radiation.[39] The polarisation of the infrared body emission is modified with the surface roughness [40] or when surmounting the material with sub-wavelength periodic gratings.[41–45]

The polarisation direction changes to perpendicular to the plane of incidence for small object sizes, the critical size of which is of the same order of magnitude than the light wavelength at which state the Fresnel terms derived under the assumption that electromagnetic radiation is reflected from a planar phase boundary of infinite extent. The degree of linear polarisation, called ρ, of thermal radiation is a monotonically increasing function of the zenithal angle, called θ, leading to a non-ambiguous relationship, $\rho(\theta)$. This property was used to disambiguate the zenithal angle of the reflected light.[5] Thus, the polarised characteristics of the thermal signature contain geometrical information of the emitting surface.

The polarimetric analysis of the emitted radiations from the weld pool free surface is determined following the method described in [46]. Three (S_0, S_1, S_2) out of the four unknown Stokes parameters of the thermal radiations are determined by interpolating the equation for each corresponding pixel in each sub-image of a linear polariser oriented at an angle α:

$$I(\alpha) = \frac{1}{2} \times (S_0 + S_1 \times \cos(2\alpha) + S_2 \times \sin(2\alpha)) \tag{1}$$

$I(\alpha)$ is light magnitude at each pixel. The degree of linear polarisation ρ is defined as:

$$\rho = \frac{\sqrt{S_1^2 + S_2^2}}{S_0} \tag{2}$$

The emissivity ε of thermal emissions is the mean value of the emissivities $\varepsilon_{//}$ and $\varepsilon_{\perp}$ of thermal emissions with a polarisation analysis direction parallel and perpendicular to the plane of incidence, respectively. These emissivities are given by [47]:

$$\begin{cases} \varepsilon_{//} = \frac{4n \times \cos(\theta)}{(n^2+k^2) \times \cos^2(\theta) + 2n \times \cos(\theta) + 1} \\ \varepsilon_{\perp} = \frac{4n \times \cos(\theta)}{\cos^2(\theta) + 2n \times \cos(\theta) + n^2 + k^2} \end{cases} \tag{3}$$

where n and k are respectively real and imaginary parts of the complex refractive index. The emergence angle θ is then inferred using the bijective relationship:

$$\rho = \frac{\varepsilon_{//} - \varepsilon_{\perp}}{\varepsilon_{//} + \varepsilon_{\perp}} = \frac{(n^2 + k^2 - 1) \times (1 - \cos^2(\theta))}{(1 + n^2 + k^2) \times (1 + \cos^2(\theta)) + 4n \times \cos(\theta)} \tag{4}$$

Once the emissivity of a radiated point has been calculated, its temperature T is calculated based upon a calibrated relationship between the measured intensity S_0 and the radiance of a blackbody at a known temperature. The relationship of the radiance of the weld pool surface L with the temperature T is given by Planck's law:

$$T = \frac{h \times c}{\lambda \times k_B \times \ln\left(1 + 2\frac{\varepsilon \times h \times c^2}{\lambda^5 \times L}\right)} \tag{5}$$

where λ is wavelength, h is Planck's constant, k_B is Boltzmann's constant, and c is speed of light. Hence the polarimetric state of radiated light permits both the thermal field and topography reconstruction.

3. Determination of the complex refractive index

The complex refractive index of the liquid weld pool is assumed temperature-independent from the melting to the boiling temperatures (i.e. from 1811 to 3134 K, respectively), that is the range of temperatures expected in the weld pool and approximated as the iron one. All possible (n, k) combinations verifying the following Equation (6) are calculated and presented in Figure 1:

$$\frac{\varepsilon_{//} + \varepsilon_{\perp}}{2} = \varepsilon \tag{6}$$

where $\varepsilon_{//}$ and $\varepsilon_{\perp}$ are calculated from Equation (3), and ε is the value for emissivity found in literature for Liquid iron, for a normal incidence, i.e. $\theta = 0°$, and for a 650 nm centred wavelength. For each (n, k) combinations, a complete temperature map is computed using Matlab programming. For the refractive index $m = n - ik = 8–2.3i$, a weld pool edge temperature (i.e. 1822 K) closest to the assumed liquidus temperature (i.e. 1811 K) is reached.

4. Experimental set-up

We have implemented our approach by using a monospectral near-infrared polarimeter associated to a stationary gas tungsten arc welding (GTAW) process. It was performed at 120 A, DCEN (Direct Current Electrode Negative), with a 4 mm-arc gap on a 200 × 200 × 20 mm^3 low-carbon steel block using pure helium shielding gas. The weld pool is observed with a GE1650 camera at a grazing angle of 23° through a 810 nm narrow bandpass filter during welding (Figure 2(a)). As the weld pool temperature ranges from the liquidus (1811 K) to the boiling point (3134 K), Wien's law estimate the peak of intensities of thermal radiation for wavelengths from 943 nm (3134 K) to 1635 nm (1811 K). Nevertheless, the 810 nm wavelength was chosen for observation because of the low absolute quantum efficiency (<0.1) above 810 nm of the camera and a blind spectral window at 810 nm of a helium plasma. Fitted on the GE1650 camera, a division of aperture polarimetric system (MultiSpec-Imager from Optical Insights

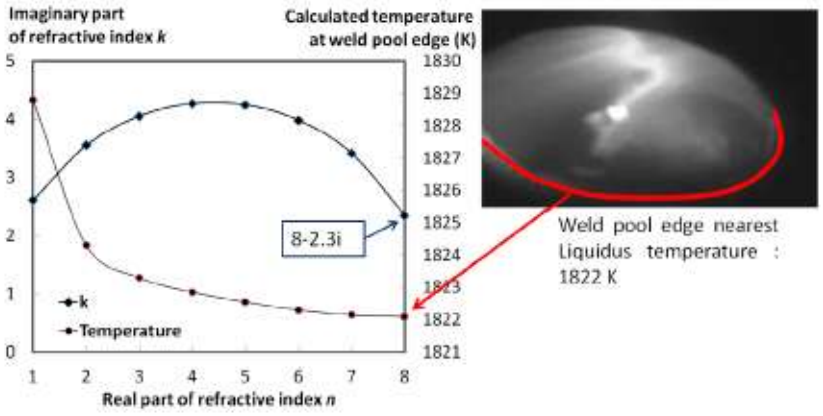

Figure 1. Range of possible refractive index (n, k) and corresponding calculated temperature at weld pool edge.

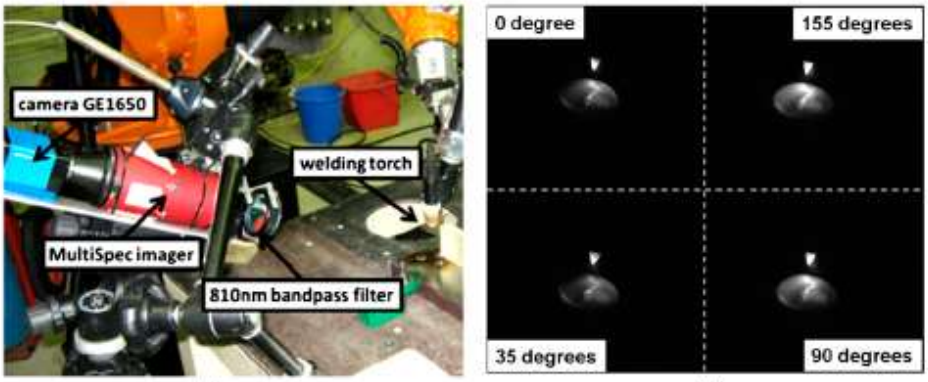

Figure 2. (a) Division of aperture polarimetric system, and (b) raw focal-plane image (1200 × 1600 pixels) showing four polarisation channels at indicated orientation.

Company based in Santa-Fe, New Mexico, USA) similar to one presented in [31] equips with four Polarcor linear polarisers 05P109AR.16 from Newport makes, simultaneously, all polarisation measurements for every pixel of the dynamic scene (Figure 2(b)). The Multispec-Imager system captures different polarisation states of an object at one single instant, thus suitable for observing dynamic scenes. The simultaneous four-imaging system avoids the need of mechanically-rotating polarisation filters ahead of a CCD-sensor camera to acquire image components at different polarisation orientations. Hence there is no more time lag between rotation steps and no shift in perspective projection of the scene onto the image plane (optical distortion).[48] In this configuration with linear polarising filters, the Multispec Imager is a partial Stokes polarimeter that evaluates the S_0, S_1 and S_2 parameters. Low intensity current was preferred to reduce background radiance of arc plasma.[1] Steel was chosen for its relatively high temperature of melting (1811 K) and consequently intense thermal radiations (Planck's law). Lens diaphragm to f/2.8, corresponding to an approximate aperture diameter of 8.93 mm, and exposure time to 2400 µs are setup.

4.1. Temperature system calibration

Calibration of the system was required to analyse quantitatively the emission. The relative grey-level attenuation coefficients of each light path (coefficients of 0.75, 1.00, 1.33, and 0.86 for sub-image at 0, 35, 90, and 155 degrees, respectively) were evaluated by acquiring an image without polarised filters and applied on the corresponding polarised sub-image. The object radiance L (W sr^{-1} m^{-2} nm^{-1}), calculated with Planck's law, was associated to the Stokes parameter S_0 by filming a heated blackbody made in ceramic $LaCrO_3$ from 473 to 1923 K inside a pyrometer calibration furnace Pyrox PY15. The blackbody diameter is 15 mm. Images of the blackbody were acquired using the camera equipped of the polarised filters and the 810 nm-bandpass filter. The exposure time and diaphragm were adjusted in similarity to the adjustments during welding observation. The parameter S_0 is calculated for each acquired image and associated to a temperature (Figure 3(a)). Considering an emissivity of 1 independent of the direction of thermal emission, the luminance of the body was estimated

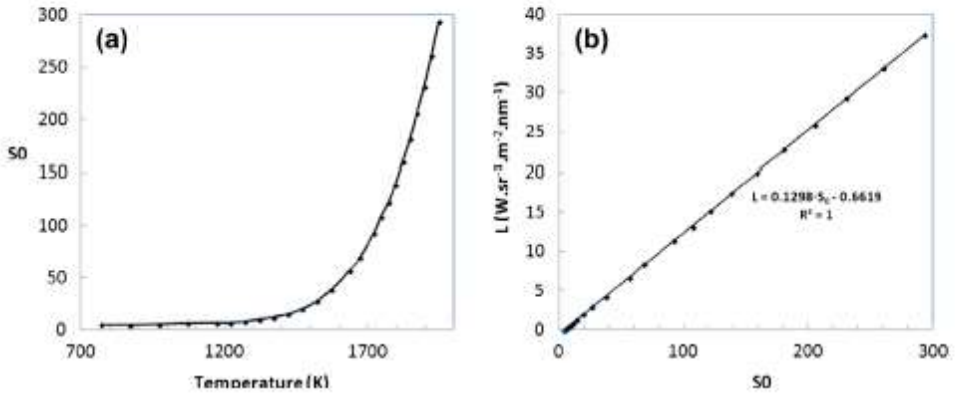

Figure 3. (a) S_0 (Stokes parameter) vs Temperature (K), (b) radiance (L) vs S_0 calculated using Planck's law, Equation (5).

from its temperature using the Planck's law. A mean value of S_0 was calculated for a 51x51 pixels region (Figure 3(b)). A linear best-fitting of the data points gives the relationship (7):

$$L = 0.1298 \times S_0 - 0.6619 \tag{7}$$

The variation of S_0 in this region was within 2% with a standard deviation below 0.7%.

4.2. *Polariser orientation calibration*

The axis of the polarisation filters relative to each other were determined using a white computer flat screen and pivoting the camera around its axis, which was perpendicular to the screen, see Figure 4. The white computer flat screen emits a linearly polarised light. Looking along the camera direction, the filters were oriented with respect to the filter axis of the top-left image at 35° (bottom-left sub-image), 90° (bottom-right sub-image), and 155° (top-right image) in a trigonometric direction. The three parameters

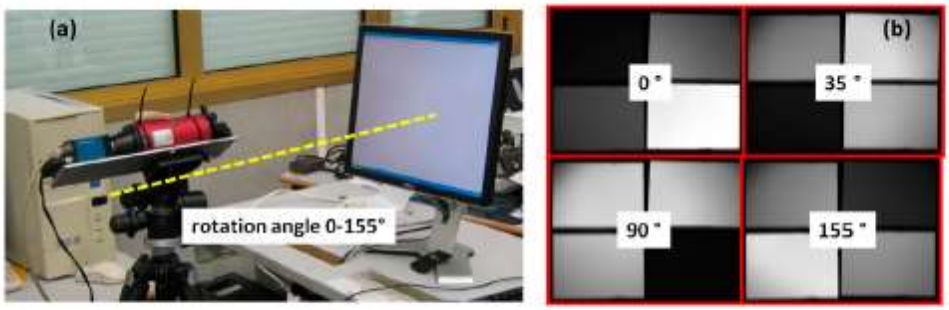

Figure 4. (a) Experimental setup for calibration of filter orientation, and (b) intensity-orientation results.

for partial linear polarisation can be derived from the four image radiances acquired under different polarising filter orientations. This calibration procedure of the entire vision system enables to account for polarisation anomalies induced by the optics.

5. Results and discussion

Infrared weld pool radiance is composed of external environment reflection, tungsten tip glints, blackbody emission from wave facets (thermally emitted radiance). The dominant radiance intensity of the weld pool and tungsten tip allows us to neglect the environment contribution. The tungsten tip glint, located on a very small zone, contributes by reflection to the polarised information but will be treated as a strong emitted light point to simplify this approach. The emission from the weld pool facets is the signal we are interested in. The emitted radiations may be affected by the transmitting medium (i.e. atmosphere) before reaching the camera sensor. The transmission through the surrounding atmosphere and emission from the helium plasma is neglected as this one does not emit significantly in the selected spectral wavelength.

Multiple reflections, in which the light reaches the detector after two or more reflections from the weld pool surface, and shadowing, in which one facet blocks the view of the facet behind it, are not accounted for. These effects become important for large capillary waves travelling along the phase boundary of the liquid metal, whose dynamics are dominated by the effects of surface tension often referred to as ripples, and for grazing camera viewpoints. GTA weld pool is performed without electrode displacement and with welding parameters generating a 'calm' surface, in particular by using a constant welding current to minimise superficial oscillations. If selecting a too-grazing path, multiple scattering and shadowing are expected to dominate single-scattering events. Hence the camera viewpoint is selected as much vertical as possible so that the tungsten tip does not physically hide parts of the weld pool.

In Figure 5, calculated images for S_0, S_1 and S_2 parameters are shown. The weld pool and the tungsten tip edges are easily identified. Some ghost-effect at the tungsten tip is believed to arise from internal reflection of the light and the intense emission of the tungsten tip at these camera adjustments. The saturation of the tungsten tip is a consequence of these camera adjustments. The weld pool emits thermal radiations with lower intensity than tungsten tip because, at high temperatures, the tip emits more light and peak is closer to 810 nm according to Wien's law. It is proven by the present images that the weld pool and tungsten tip are glowing objects emitting energy in the

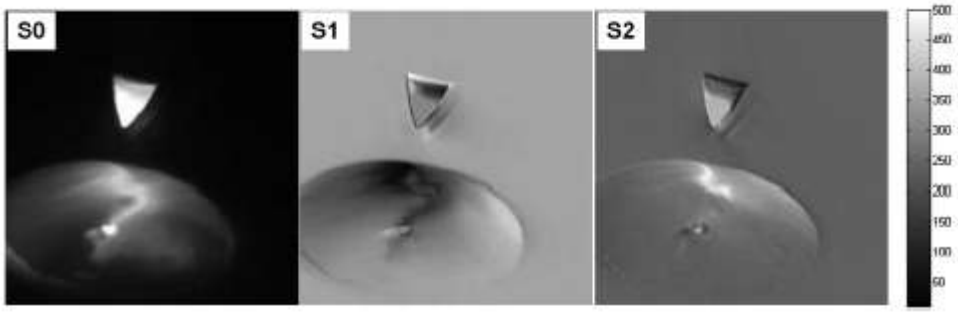

Figure 5. S_0, S_1 and S_2 parameters are calculated. Background values are not relevant.

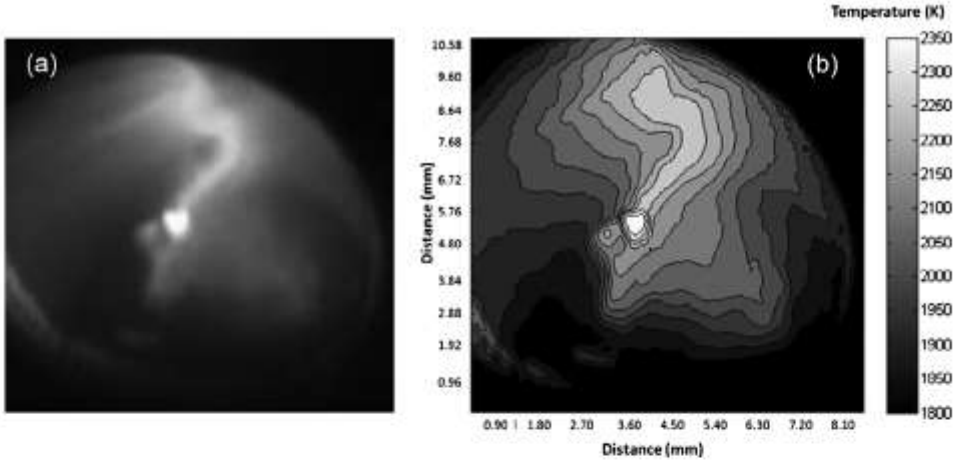

Figure 6. (a) Convex weld pool, and (b) calculated thermal field at the surface.

810 nm wavelength during GTAW process. ρ, i.e. degree of linear polarisation is calculated from the S_0, S_1 and S_2 Stokes parameters. Then, θ, i.e. zenithal angle, is determined using Equation (4).

The brightest zone in Figure 6(a), at a temperature estimated above 2367 K in (b), is due to oxide aggregate floating at weld pool surface. The hot spot stays at the weld pool centre for convex welds but wanders along the weld pool edge for concave welds. Oxide aggregate is formed, progressively, during welding performance by accumulation of smaller oxide particles. Most of them formed at the solid edge of the weld pool that is at high temperature and are brought into the weld pool by the expansion (i.e. increasing diameter) of it. The heating spot is observed to stick to the oxide island preferentially. The oxides move under the complex action of the Marangoni flow, shielding gas flow, and arc pressure. The bright lines emerging from this hot spot (Figure 6(a)) are visible in the reconstructed thermal field (Figure 6(b)) and may be hot liquid flowing away from this zone due to Marangoni convection phenomenon.

6. Conclusion

In opposite to the work of Kraus et al., our method does not require assumptions with respect to the dependence of emissivity on direction. Compared to polychromatic or bichromatic measurement methods, our method does not need to assume that emissivity is independent from wavelength within the two or more used spectral bands. The method is usable during welding process, and is fast enough to be sensitive to weld pool dynamic behaviour.

The polarimetry of thermal radiations permits a dense reconstruction of the thermal field occurring on weld pool surfaces. Nevertheless, sources of errors must be identified prior to technological developments. Among those likely error sources are the background emission of arc plasma (see our recent work in [48]), the floating oxides emitting at different emissivities and temperatures and the lack of knowledge concerning optical properties of metallic liquid surface. Also, the lack of knowledge about undercooling temperature of metal induces a source of error for a precise determination of

complex refractive index. The postulate that liquid iron normal emissivity is wavelength independent in the range 650–810 nm can be a source of error, better estimation of the emissivity is necessary.

A more universal observation window must be found in the infrared region. The technological innovations should be extendable to other welding processes, i.e. MIG, Plasma, Laser and even other applications. The thermal field visualisation will inform on the surface Marangoni flows. The shape and thermal field of MIG droplets could be determined. An innovative process may follow to control assembling processes and to perform non-contact dimensional control. It may be included to quality control of industrial systems.

Acknowledgement

The authors acknowledge the *Conseil Régional de Bourgogne* for the financial support of this work.

Disclosure statement

No potential conflict of interest was reported by the authors.

References

[1] Weglowski MS. Investigation on the arc light spectrum in GTA welding. JAMME. 2007;20:519–522.
[2] Abdullah BM. Monitoring of welding using Laser diodes. In: Dnyaneshwar SP, editor. Semiconductor Laser diode technology and applications. Rijeka: InTech; 2012. p. 241–262. Available from: http://www.intechopen.com/books/semiconductor-laser-diode-technology-and-applications/monitoring-of-welding-using-laser-diodes.
[3] Huang RS, Liu LM, Song G. Infrared temperature measurement and interference analysis of magnesium alloys in hybrid laser-TIG welding process. Mater. Sci. Eng. A. 2007;447:239–243.
[4] Zhang G, Wu CS, Liu Z. Experimental observation of both keyhole and its surrounding thermal field in plasma arc welding. Int. J. Heat Mass Transfer. 2014;70:439–448.
[5] Miyazaki D, Saito M, Sato Y, et al. Determining surface orientations of transparent objects based on polarization degrees in visible and infrared wavelength. J. Opt. Soc. Am. A. 2002;19:687–694.
[6] Bimonte G, Cappellin L, Carugno G, et al. Polarized thermal emission by thin metal wires. New J. Phys. 2009;11. Article ID: 033014 (p. 11).
[7] Lukens W, Morris R, Dunn E. IR temperature sensing of cooling rates for arc welding control. DTNSRDC/SME-80/70. Bethesda (MD); 1981; p. 20084.
[8] Doong JL, Wu CS, Hwang JR. Infrared temperature sensing of laser welding. Int. J. Mach. Tools Manuf. 1991;31:607–616.
[9] Moreira P, Frazão O, Tavares S, et al. Temperature field acquisition during gas metal arc welding using thermocouples, thermography and fibre Bragg grating sensors. Meas. Sci. Technol. 2007;18:877–883.
[10] Liang G, Yuan S. Study on the temperature measurement of AZ31B magnesium alloy in gas tungsten arc welding. Mater. Lett. 2008;62:2282–2284.
[11] Liu L, Chi M, Huang R, et al. Infrared measurement and simulation of magnesium alloy welding temperature field. Sci. China Ser. E. 2005;48:706–715.
[12] Boillot J, Cielo P, Begin G, et al. Adaptive welding by fiber optic thermographic sensing: an analysis of thermal and instrumental considerations. Weld. J.: Weld. Res. Suppl. 1985:209s–218s.
[13] Matteï S, Grevey D, Mathieu A, et al. Using infrared thermography in order to compare laser and hybrid (laser+MIG) welding processes. Opt. Las. Technol. 2009;41:665–670.

[14] Mathieu A, Matteï S, Deschamps A, et al. Temperature control in laser brazing of a steel/aluminium assembly using thermographic measurements. NDT and E Int. 2006;39:272–276.
[15] Chin D, Madsen N, Goodling J. Infrared thermography for sensing the arc welding process. Weld. J.: Weld. Res. Suppl. 1983:227s–234s.
[16] Nagajaran S, Chen W, Chin B. Infrared sensing for adaptive arc welding. Weld. J.: Weld. Res. Suppl. 1989:462s–466s.
[17] Chen W, Chin B. Monitoring joint penetration using infrared sensing techniques. Weld. J.: Weld. Res. Suppl. 1990:181s–185s.
[18] Bicknell A, Smith J, Lucas J. Infrared sensor for top face monitoring of weld pools. Meas. Sci. Technol. 1994;5:371–378.
[19] Bertrand P, Smurov I, Grevey D. Application of near infrared pyrometry for continuous Nd: YAG laser welding of stainless steel. Appl. Surf. Sci. 2000;168:182–185.
[20] Doubenskaia M, Bertrand P, Smurov I. Pyrometry in laser surface treatment. Surf. Coat. Technol. 2009;201:1955–1961.
[21] Bertrand P, Ignatiev M, Flamant G, et al. Pyrometry applications in thermal plasma processing. Vacuum. 2000;56:71–76.
[22] Tanaka M, Waki K, Tashiro S, et al. Visualizations of 2D temperature distribution of molten metal in arc welding process. T. JWRI. 2009;38:1–4.
[23] Siewert E, Schein J, Forster G. Determination of enthalpy, temperature, surface tension and geometry of the material transfer in PGMAW for the system argon–iron. J. Phys. D Appl. Phys. 2013;46:224008.
[24] Shöpp H, Sperl A, Kozakov R, et al. Temperature and emissivity determination of liquid steel S235. J. Phys. D: Appl. Phys. 2012;45:235203.
[25] Kozakov R, Schöpp H, Gött G, et al. Weld pool temperatures of steel S235 while applying a controlled short-circuit gas metal arc welding process and various shielding gases. J. Phys. D: Appl. Phys. 2013;46:475501.
[26] Kraus H. Optical spectral radiometric method for measurement of weld pool surface temperatures. Opt. Lett. 1986;11:773–775.
[27] Kraus H. Experimental measurement of stationary SS 304, SS 316L and 8630 GTA weld pool surface temperatures. Weld. J.: Weld. Res. Suppl. 1989:269s–279s.
[28] Klein L, Ingvarsson S, Hamann H. Changing the emission of polarized thermal radiation from metallic nanoheaters. Opt. Express. 2009;17:17963–17969.
[29] Weast RC. CRC handbook of chemistry and physics. 69th ed; Boca Raton (FL): CRC Press Inc; 1988. E-405.
[30] Coniglio N, Mathieu A, Aubreton O, et al. Characterizing weld pool surfaces from polarization state of thermal emissions. Opt. Lett. 2013;38:2086–2088.
[31] Tyo JS, Goldstein D, Chenault D, et al. Review of passive imaging polarimetry for remote sensing applications. Appl. Opt. 2006;45:5453–5469.
[32] Klein L, Hamann H, Au Y, et al. Coherence properties of infrared thermal emission from heated metallic nanowires. Appl. Phys. Lett. 2008;92:213102–213106.
[33] Yannopapas V. Effect of material spatial dispersion in the degree of polarization of thermal radiation emitted by a spherical source. Opt. Commun. 2010;283:4494–4498.
[34] Ingvarsson S, Klein L, Au Y, et al. Enhanced thermal emission from individual antenna-like nanoheaters. Opt. Express. 2007;15:11249–11254.
[35] Hesketh P, Zemel J, Gebhart B. Polarized spectral emittance from periodic micromachined surfaces. I. Doped silicon: the normal direction. Phys. Rev. B. 1988;37:10795–10802.
[36] Hesketh P, Zemel J, Gebhart B. Polarized spectral emittance from periodic micromachined surfaces. II. Doped silicon: angular variation. Phys. Rev. B. 1988;37:10803–10813.
[37] Marquier F, Joulain K, Mulet J, et al. Coherent spontaneous emission of light by thermal sources. Phys. Rev. B. 2004;69:155412.
[38] Bertilone D. Stokes parameters and partial polarization of far-field radiation emitted by hot bodies. J. Opt. Soc. Am. A. 1994;11:2298–2304.
[39] Rahmann S, Canterakis N. Reconstruction of specular surfaces using polarization imaging. IEEE. Proceedings of the conference on Computer Vision and Pattern Recognition; Kauai Marriott (HI): IEEE Computer Society; 2001.
[40] Worthing A. Deviation from Lambert's law and polarization of light emitted by incandescent tungsten, tantalum and molybdenum and changes in the optical constants of tungsten with temperature. J. Opt. Soc. Am. A. 1926;13:635–647.

[41] Jordan D, Lewis G. Measurements of the effect of surface roughness on the polarization state of thermally emitted radiation. Opt. Lett. 1994;19:692–694.
[42] Lee JH, Lee JCW, Leung W, et al. Polarization engineering of thermal radiation using metallic photonic crystals. Adv. Mater. 2008;20:3244–3247.
[43] Lee JH, Leung W, Kim T, et al. Polarized thermal radiation by layer-by-layer metallic emitters with sub-wavelength grating. Opt. Express. 2008;16:8742–8747.
[44] Dahan N, Niv A, Biener G, et al. Thermal image encryption obtained with a SiO_2 space-variant subwavelength grating supporting surface phonon-polaritons. Opt. Lett. 2005;30:3195–3197.
[45] Dahan N, Niv A, Biener G, et al. Space-variant polarization manipulation of a thermal emission by a SiO_2 subwavelength grating supporting surface phonon-polaritons. Appl. Phys. Lett. 2005;86:191102.
[46] Wilkie A, Weidlich A. A physically plausible model for light emission from glowing solid objects. Comput. Graph. Forum. 2011;30:1269–1276.
[47] Gurton KP, Dahmani R, Videen G. Measured degree of infrared polarization for a variety of thermal emitting surfaces. U.S. Army Research Lab. ARL-TR-3240. Adelphi (MD); 2004.
[48] Coniglio N, Mathieu A, Aubreton O, et al. Plasma effect on weld pool surface reconstruction by shape-from-polarization analysis. Appl. Phys. Lett. 2014;104:131603.